

Synthesis, crystal structure, and near-infrared reflective properties of $\text{ZnS}_x\text{Se}_{1-x}$ nanopigments

Ti Zhang^{a,b}, Yanmin Wang^{a,*}, Shanjun Ke^{b,*} and Zhidong Pan^a

^aSouth China University of Technology, Guangzhou 510640, China

^bFoshan Oceano Ceramics Co. Ltd., Foshan 528138, China

In this research, a series of near-infrared (NIR) reflecting nanopigments, based on $\text{ZnS}_x\text{Se}_{1-x}$ ($x = 1, 0.75, 0.55, \text{ and } 0.35$), have been synthesized *via* a coprecipitation reaction and subsequent calcination. Furthermore, their crystal structure, particle morphology, chromatic properties, and NIR reflectance have been investigated in detail; the results show that $\text{ZnS}_x\text{Se}_{1-x}$ pigments have a cubic zinc-blende structure with a space group of $F-43m(216)$, and the pigments' microstructure presents the agglomerates composed of the spherical particles of different nanosizes. $\text{ZnS}_x\text{Se}_{1-x}$ pigments exhibit not only colors ranging from ivory white to bright yellow but also significant NIR solar reflectance, ranging from 80.96% to 86.65%.

Keywords: $\text{ZnS}_x\text{Se}_{1-x}$, Coprecipitation, Near-infrared reflectance, Cool pigment.

Introduction

Currently, due to the urban heat-island effect [1], temperatures in city centers are 3 °C–5 °C higher than in the surroundings. As the urban buildings absorb sunlight, the indoor temperatures increase, affecting people's living comfort and increasing the building cooling energy consumption. Over the next three decades, the urban heat-island phenomenon is expected to become increasingly severe; at the same time, the energy consumption related to this phenomenon is estimated to increase with the deterioration of the ecological environment and the climate. Therefore, the implementation of urban heat-island mitigation strategies in the next few years will be crucial. In the past few decades, "cool pigments" with high solar reflectance have attracted a broad audience [2, 3]; furthermore, several inorganic pigments with high NIR reflectance have been developed to address this issue [4, 5].

The solar/NIR reflectance of inorganic pigments [6] are closely related to its color. White pigments, e.g., TiO_2 [7] and ZnO [8], have excellent thermal reflection properties (total solar reflectance of approximately 85%). However, due to the poor stain resistance of white coatings, it is necessary to develop a variety of NIR reflective pigments with different colors that can simultaneously meet the aesthetics, antiglare, and anti-fouling properties, so as to meet people's many needs for product functionality and practical beauty [9–19].

Recently, zinc selenide sulfide ($\text{ZnS}_x\text{Se}_{1-x}$) materials have emerged as promising materials for environmental and energy applications. $\text{ZnS}_x\text{Se}_{1-x}$ is a continuous solid solution of two compounds, zinc sulfide [20–24] and zinc selenide, and its band-gap value shows a continuous change with the composition x . As a wide-bandgap II–VI semiconductor material with high photostability and luminescence quantum yield potential, $\text{ZnS}_x\text{Se}_{1-x}$ has been widely studied in the fields of light-emitting devices, solar cells, sensors, and optical recording materials. However, there are still few reports on the preparation of $\text{ZnS}_x\text{Se}_{1-x}$ as high NIR reflection inorganic pigments. Although our previous work found that $\text{ZnS}_x\text{Se}_{1-x}/\text{ZrSiO}_4$ composite can be used as a cool pigment on ceramic tiles for energy saving, the formation mechanism of $\text{ZnS}_x\text{Se}_{1-x}$ "cool pigment" is still unknown and the research on the color and the thermal performance of $\text{ZnS}_x\text{Se}_{1-x}$ are not systematic enough.

In this paper, we have synthesized a series of NIR-reflecting nanopigments based on zinc selenide sulfide ($\text{ZnS}_x\text{Se}_{1-x}$, $x = 1, 0.75, 0.55, \text{ and } 0.35$) and a solid solution whose composition changes with the x component ratio [25] *via* a coprecipitation reaction and subsequent calcination. Furthermore, we have analyzed the crystal structure, valence state, morphology, chromaticity, and NIR reflective properties of the same.

Experimental

Materials and methods

$\text{ZnS}_x\text{Se}_{1-x}$ pigments ($x = 1, 0.75, 0.55, \text{ and } 0.35$) have been synthesized by a coprecipitation reaction and subsequent calcination (Fig. 1) using $\text{ZnSO}_4 \cdot 7\text{H}_2\text{O}$ (99.5%), $\text{Na}_2\text{S} \cdot 9\text{H}_2\text{O}$ (98%), Se (99%), and NaOH

*Corresponding author:

Tel : +86 20 87114883

Fax: +86 20 87110273

E-mail: wangym@scut.edu.cn (Y. Wang), sjkescut@163.com (S. Ke)

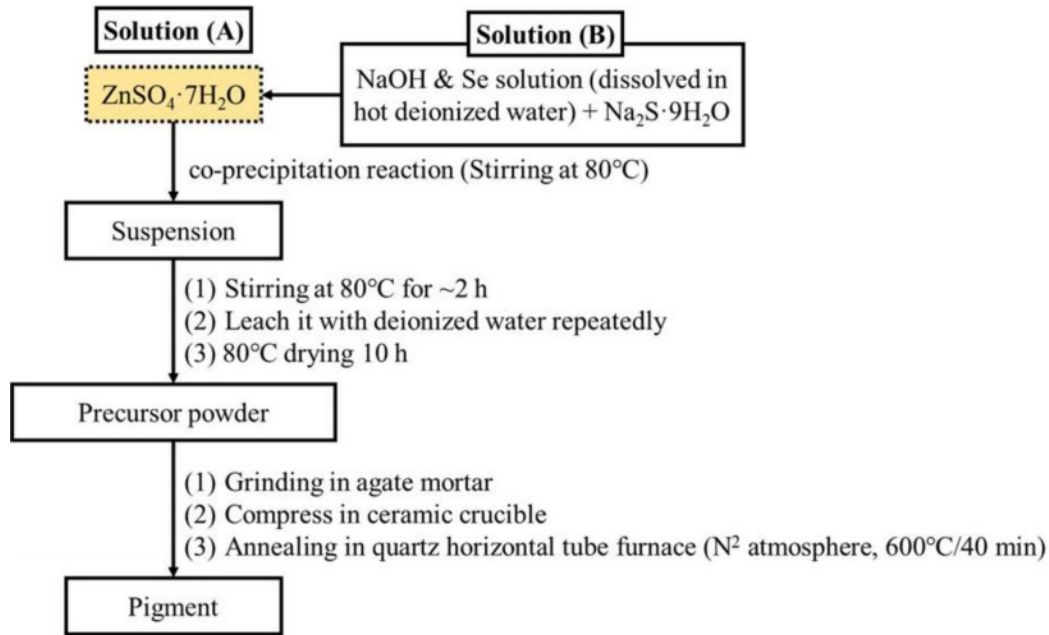


Fig. 1. Flowchart for synthesis procedure of $\text{ZnS}_x\text{Se}_{1-x}$ pigments.

Table 1. Compositions of $\text{ZnS}_x\text{Se}_{1-x}$ precursors

Sample	Precursor atomic ratio Zn:S:Se	
ZnS	1:1:0	
$\text{ZnS}_x\text{Se}_{1-x}$	ZS-0.75	1:0.75:0.25
	ZS-0.55	1:0.55:0.45
	ZS-0.35	1:0.35:0.65

(97%) as starting materials, which have been supplied by the Sinopharm Group Co. Ltd., China. Regarding the compositions of $\text{ZnS}_x\text{Se}_{1-x}$ precursors, the x value is noted to change (Table 1).

Characterizations

Crystalline phases of samples were examined through an X-ray diffractometer (PW-1710, Philips Co. Ltd., The Netherlands); the elements' valence state was determined using an X-ray photoelectron spectroscopy (ESCALAB 250Xi, Thermo Fisher Scientific Co. Ltd., USA); the samples' morphology was examined through a scanning electron microscope (EVO-18, Carl Zeiss AG, Germany); the particle size distributions were determined by a laser diffraction particle size analyzer (BT-9300S, Bettersize Instruments Ltd., China); specific surface areas of samples were determined based on the nitrogen gas adsorption principle (BET) (Flowsorb III 2310, Micrometrics Co. Ltd., USA); and the samples' color was determined on a reflection differential colorimeter (Color Premier 8200, X-Rite Incorporated, USA). Furthermore, the diffuse reflectance of samples was measured through a UV-vis-NIR spectrophotometer (LAMBDA 950, PerkinElmer Co. Ltd., USA), using BaSO_4 as a reference. The solar reflectance in the NIR region (R^*) can be calculated by:

$$R^* = \frac{\int_{700}^{2500} r(\lambda) i(\lambda) d(\lambda)}{\int_{700}^{2500} i(\lambda) d(\lambda)}, \quad (1)$$

where $r(\lambda)$ is the spectral reflectance ($\text{W}\cdot\text{m}^{-2}$), and $i(\lambda)$ is the standard solar spectrum ($\text{W}\cdot\text{m}^{-2}\cdot\text{nm}^{-1}$) obtained from the ASTM standard G159-98.

Results and Discussion

Powder X-ray diffraction analysis

Fig. 2(a) shows XRD patterns of $\text{ZnS}_x\text{Se}_{1-x}$ ($x = 1, 0.75, 0.55,$ and 0.35) composite pigments. Comparing the standard JCPDS File of ZnS (JCPDS card No. 05-0566) with that of ZnSe (JCPDS card No. 37-1463), we found that they have the same cubic zinc-blende (zb) structure with a space group of F-43m(216). The zb-ZnS shows characteristic features at $28.6^\circ, 33.1^\circ,$ and 56.3° , corresponding to (111), (220), and (311) planes, respectively. Similarly, zb-ZnSe shows characteristic features at $27.2^\circ, 31.5^\circ,$ and 45.2° , respectively, corresponding to the same planes. As the Se content further increases, the samples begin to show peaks of zb-ZnSe (JCPDS card No. 37-1463, cell parameters of $a = 5.669 \text{ \AA}$). Fig. 2(b) and Fig. 2(c) show the shifts of the Bragg reflections (111) and (220) of $\text{ZnS}_x\text{Se}_{1-x}$ powders; these are due to changes in the cell volume of $\text{ZnS}_x\text{Se}_{1-x}$ pigments. The ionic radius of Se^{2-} (1.91 \AA) is greater than that of S^{2-} (1.84 \AA) on the tetrahedral sites. When S^{2-} is substituted by Se^{2-} , the bond length of Zn-Se is less than that of Zn-S. On the contrary, when the Se content in $\text{ZnS}_x\text{Se}_{1-x}$ increases, (111) and (220) planes shift toward lower 2θ values, increasing the lattice parameters.

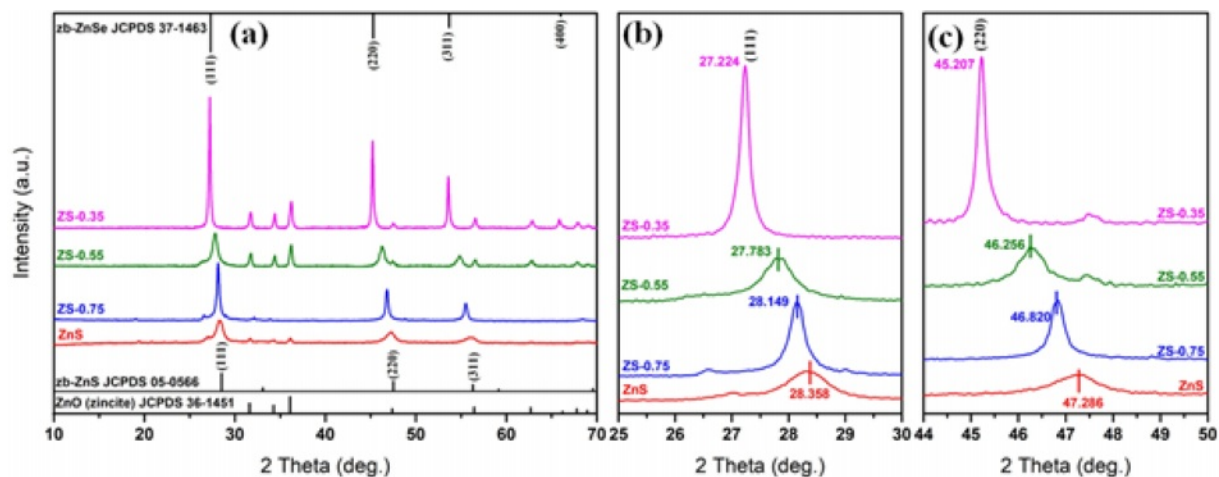


Fig. 2. (a) XRD patterns of $\text{ZnS}_x\text{Se}_{1-x}$ ($x = 1, 0.75, 0.55,$ and 0.35) pigments; (b) Bragg reflection shifts for (111) plane; and (c) for (220) plane.

Valence state analysis

Fig. 3 shows the XPS spectra of the $\text{ZnS}_x\text{Se}_{1-x}$ ($x = 0.35$) pigment, while Fig. 3(b) shows the high-resolution Zn 2p electron region. The binding energy interval 1022.1 and 1045.14 eV, and that between Zn 2p_{3/2} and Zn 2p_{1/2} are characteristic of a Zn²⁺ oxidation state [26]. The chemical state of S 2p is shown in Fig. 3(c). The peak at 160.27 eV is ascribed to S 2p_{3/2}, which is in agreement with the 160–164 eV scope attained for S in the sulfide phase [27]. The locations of the major peaks (54.04 and 54.79 eV) represent Se 3d_{3/2} and Se

3d_{1/2}, respectively, indicating that element Se mainly exists as a chemical state of Se²⁻ [28], as shown in Fig. 3(d).

Particle size and morphological analysis

Fig. 4 shows the SEM micrographs of $\text{ZnS}_x\text{Se}_{1-x}$ pigments. The result shows that the increase of Se content in $\text{ZnS}_x\text{Se}_{1-x}$ does not significantly change the samples morphology, which are granular and have a relatively uniform size distribution (see Fig. 5). However, the samples' microstructure presents agglomerates

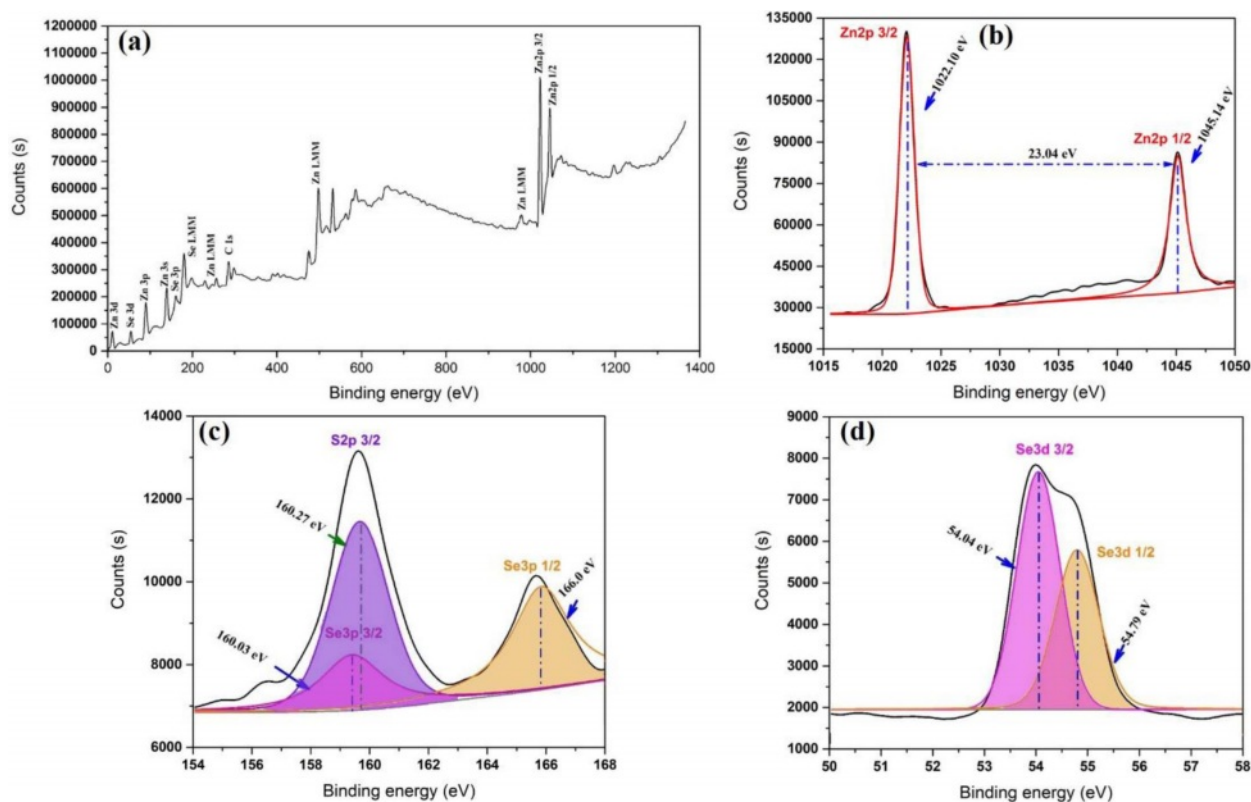


Fig. 3. XPS spectra of (a) Survey scan; (b) Zn 2p; (c) S 2p; and (d) Se 3d for the $\text{ZnS}_x\text{Se}_{1-x}$ ($x = 0.35$) pigment.

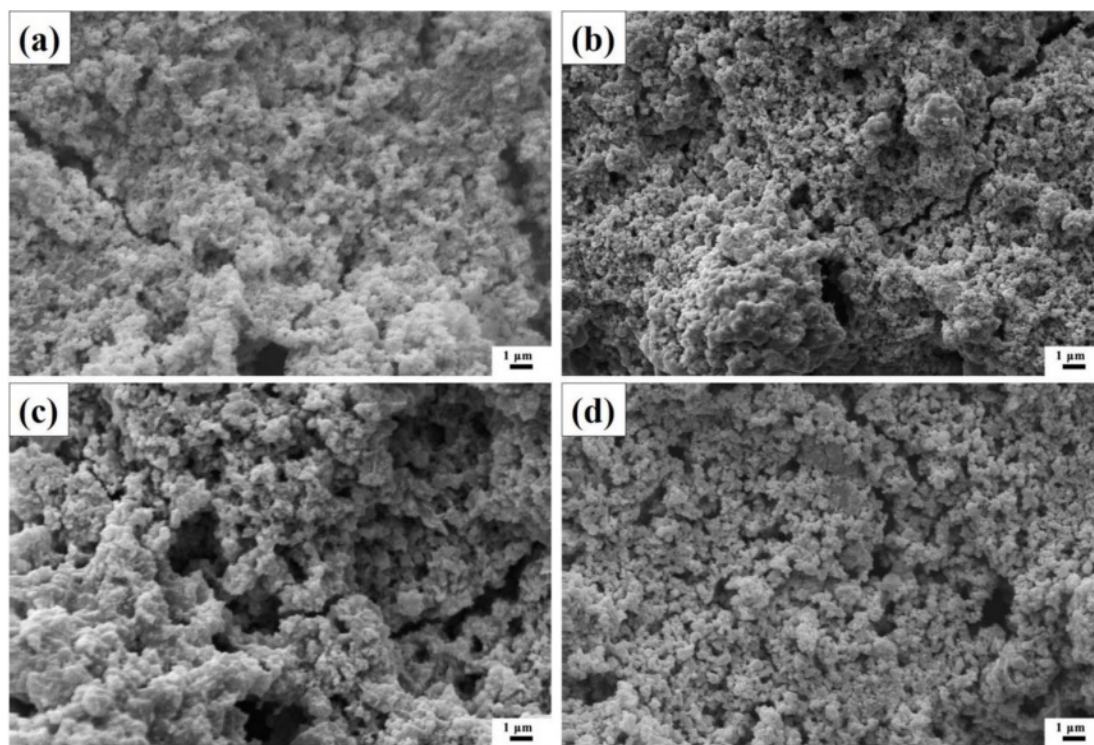


Fig. 4. SEM micrographs of $\text{ZnS}_x\text{Se}_{1-x}$ pigments: (a) ZnS; (b) ZS-0.75; (c) ZS-0.55; and (d) ZS-0.35.

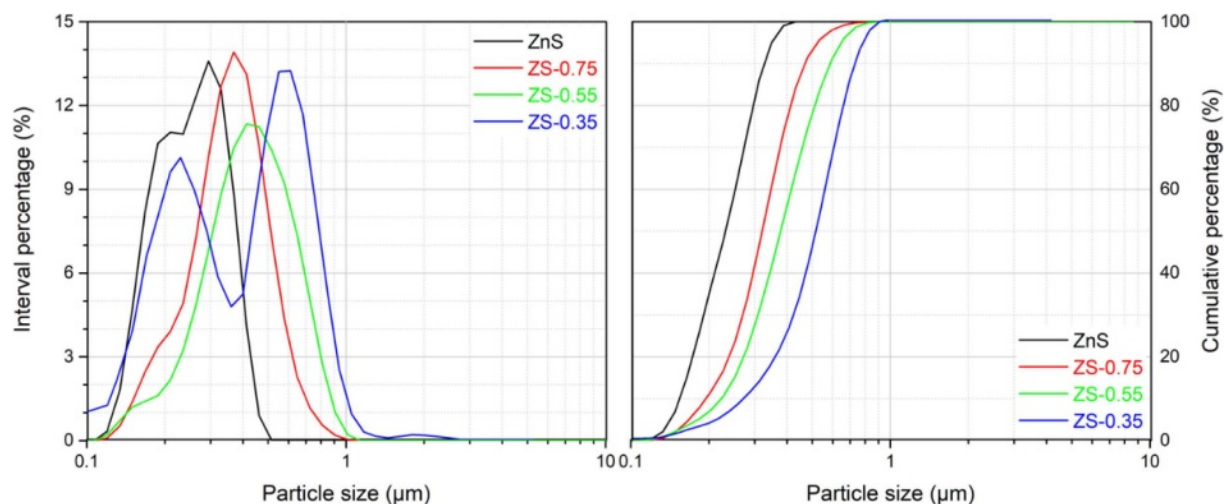


Fig. 5. Particle size distributions of $\text{ZnS}_x\text{Se}_{1-x}$ pigments.

Table 2. Specific surface areas of $\text{ZnS}_x\text{Se}_{1-x}$ pigments

Samples	ZnS	ZS-0.75	ZS-0.55	ZS-0.35
Specific surface area (m^2/g)	8.14 ± 0.03	7.68 ± 0.03	6.23 ± 0.03	5.27 ± 0.03

composed of spherical particles of different nanosizes.

The specific surface areas of $\text{ZnS}_x\text{Se}_{1-x}$ pigments are shown in Table 2. According to the BET test results, the specific surface area of the ZnS sample is $8.14 \pm 0.03 \text{ m}^2/\text{g}$. As the x value decreases, the specific surface area of $\text{ZnS}_x\text{Se}_{1-x}$ pigments gradually decreases to $5.27 \pm 0.03 \text{ m}^2/\text{g}$ ($x = 0.35$).

Chromatic properties analysis

Fig. 6 shows photographs of as-synthesized $\text{ZnS}_x\text{Se}_{1-x}$ pigments with different component ratios ($x = 1, 0.75, 0.55,$ and 0.35) by calcination in an N_2 atmosphere at $600 \text{ }^\circ\text{C}$. The visual color of calcined powders varies from ivory white to bright yellow with the variation of the component ratio.

Fig. 7 shows the chromaticity coordinates of



Fig. 6. As-synthesized ZnS_xSe_{1-x} pigments.

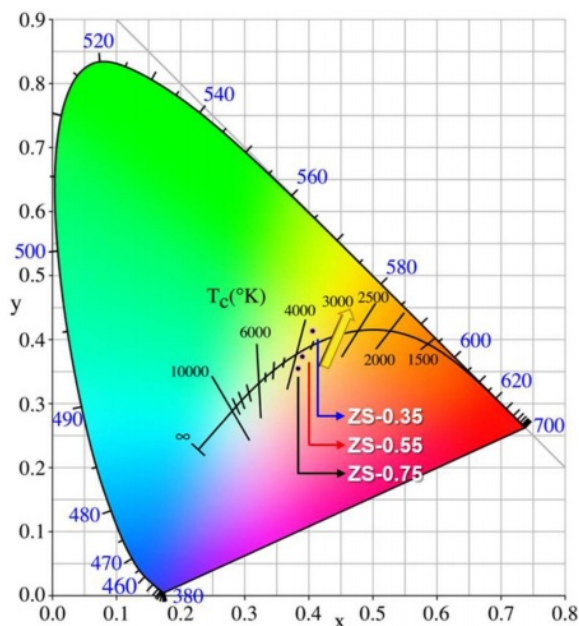


Fig. 7. Chromaticity coordinates of ZnS_xSe_{1-x} pigments.

ZnS_xSe_{1-x} pigments: these are gradually close to yellow with increasing Se content, which is consistent with the fact that the samples' color changes from ivory white to bright yellow.

Table 3 shows the influence of the x component ratio on L^* , a^* , and b^* ZnS_xSe_{1-x} parameters. As the x value

Table 3. L^* , a^* , and b^* parameters of ZnS_xSe_{1-x} pigments

Samples	L^*	a^*	b^*
ZS-0.75	67.58	12.57	33.57
ZS-0.55	61.21	10.18	31.15
ZS-0.35	81.85	12.54	56.58

decreases, brightness (L^*) increases from 67.58 to 81.85. The yellow chromaticity (b^*) of the samples depends on the degree of Se^{2-} substituting S^{2-} . With the increase of Se content, the b^* value consistently increases from 33.57 to 56.58, indicating that the yellowness of the sample is enhanced.

NIR reflectance

Fig. 8 shows NIR reflectance and solar reflectance of ZnS_xSe_{1-x} pigments. The former are greater than 80% in the wavelength range of 700–2,500 nm (Fig. 8(a)). With the increase of Se content, the R^* of ZnS_xSe_{1-x} pigments increased from 80.96% to 86.65%, while the TSR increased from 65.30% to 71.1% (Fig. 8(b)).

Table 4 shows the comparison of color and NIR reflectance value of ZnS_xSe_{1-x} pigments, taking into account data from past researches [29–35]. The ZnS_xSe_{1-x} ($x = 0.75, 0.55, 0.35$) pigments show a good color rendering and excellent NIR reflection performance. With the increase of Se content, the yellowness of the ZnS_xSe_{1-x} pigments increases significantly along with the NIR reflectance.

Conclusions

To develop the color-tunable inorganic pigments with high NIR reflectance, this paper synthesizes nanopigments based on ZnS_xSe_{1-x} ($x = 1, 0.75, 0.55,$ and 0.35) via a coprecipitation reaction and subsequent calcination. The visual color of calcined ZnS_xSe_{1-x} powder varies from ivory white to bright yellow with the variation of the component ratio. Moreover, the

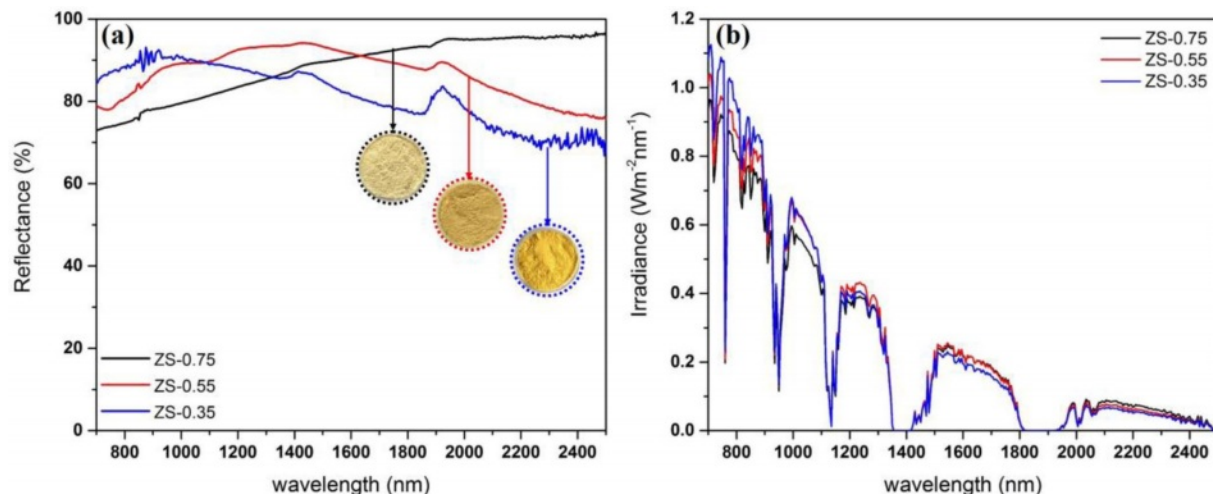












Fig. 8. (a) NIR reflectance and (b) NIR solar reflectance of ZnS_xSe_{1-x} pigments.

Table 4. Comparison of color and NIR reflectance value of ZnS_xSe_{1-x} pigments, taking into account data from past researches

Pigment	Color	NIR reflectance (%)	Ref.
Y _{4-x} Zr _x MoO _{9+δ}		83–90	[29]
Y _{4-x} A _x MoO _{9+δ} (A = Ta, Tb)		70–90	[30]
[(LiRE) _{0.125} Bi _{0.75}][W _{0.25} V _{0.75}]O ₄ (RE = La-Yb)		89–91	[31]
Sr ₂ M _{1-x} Tb _x O ₄ (M = Sn, Zr)		91–95	[32]
Bi _{1.7} RE _{0.3} W _{0.7} Mo _{0.3} O ₆ (RE = Y, Yb, Gd, Lu)		80–96	[33]
BiV _{1-x} M _x O ₄ (M=Ta, P)		81–91	[34]
[(LiLaZn) _{x/3} Bi _{1-x}][Mo _x V _{1-x}]O ₄		70–88	[35]
ZnS _x Se _{1-x}		80.96	This study
(x = 0.75, 0.55, and 0.35)		86.09	
		86.65	

samples of ZnS_xSe_{1-x} (x = 0.75, 0.55, and 0.35) possess higher NIR reflectance in the range of 80.96–86.65 at 700–2500 nm. As the x value decreases, brightness (L*) increases from 67.58 to 81.85. With the increase of Se content, the yellow chromaticity (b*) value consistently increases from 33.57 to 56.58, indicating the excellent yellow properties of ZS-0.35 pigment. Based on the NIR reflectance and various color hues obtained, the ZnS_xSe_{1-x} nanopigments could have an application as excellent candidates for “cool pigments.”

Acknowledgements

This work was supported by the China Postdoctoral Science Foundation (No. 2021M690722) and Guangdong Basic and Applied Basic Research Foundation (No. 2021A1515110487).

References

- M. Ullah, H.J. Kim, J.G. Heo, D.K. Roh, and D.S. Kim, *J. Ceram. Process. Res.* 20 (2019) 86-91.
- A. Synnefa, M. Santamouris, and K. Apostolakis, *Sol. Energy* 81 (2007) 488-497.
- M. Suwan, P. Premjit, P. Thavorniti, P. Kidkhunthod, and S. Supothina, *J. Ceram. Process. Res.* 18 (2017) 10-15.
- P. Meenakshi and M. Selvaraj, *Sol. Energy Mater. Sol. Cells* 174 (2018) 530-537.
- Y. Shi, M. Zhong, Z. Zhang, and D. Wang, *Ceram. Int.* 43 (2017) 5979-5983.
- J.H. Lee, H.J. Hwang, J.W. Kwon, J.H. Kim, K.T. Hwang, and K.S. Han, *J. Ceram. Process. Res.* 20 (2019) 127-132.
- R. Azizi, S. Rasouli, N.P. Ahmadi, A.J.J. Kolaei, and M. Azizie, *J. Ceram. Process. Res.* 13 (2012) 164-169.
- T.N. Rao, I. Hussain, Riyazuddin, and B.H. Koo, *J. Ceram. Process. Res.* 20 (2019) 411-417.
- L.L. Wang, X.X. Liu, X.P. Li, X.F. Wang, L.N. Feng, and X.R. Hou, *J. Ceram. Process. Res.* 22 (2021) 240-245.
- J. Zhang, Y.M. Park, X.Y. Tan, M.K. Bae, D.J. Kim, T.H. Jang, M.S. Kim, S.W. Lee, and T.G. Kim, *J. Ceram. Process. Res.* 20 (2019) 589-596.
- S. Jamshidi, S. Rasouli, B. Janipour, and B. Mirhadi, *J. Ceram. Process. Res.* 16 (2015) 667-673.
- W. Chatjuthamane, R. Muanghlua, B. Boonchom, and N. Vittayakorn, *J. Ceram. Process. Res.* 13 (2012) 713-716.
- B. Tanisan and S. Turan, *J. Ceram. Process. Res.* 12 (2011) 462-467.
- S. Rasouli, M. Valefi, S.J. Moeen, and A.M. Arabi, *J. Ceram. Process. Res.* 12 (2011) 450-455.
- S. Rasouli, *J. Ceram. Process. Res.* 12 (2011) 668-672.
- K.-R. Pyon, K.-S. Han, and B.-H. Lee, *J. Ceram. Process. Res.* 12 (2011) 279-288.
- Y.Z. Halefoglul and E. Kusvuran, *J. Ceram. Process. Res.* 11 (2010) 92-95.
- N. Gurbuz, E. Coskun, and E. Ozel, *J. Ceram. Process. Res.* 11 (2010) 184-190.
- H.S. Lee and B.H. Lee, *J. Ceram. Process. Res.* 9 (2008) 286-291.
- S.D. Yoon, J.W. Yun, and Y.H. Yun, *J. Ceram. Process. Res.* 21 (2020) 479-487.
- X. Tian, Z. Chen, J. Wen, Y. Du, J. Hu, S. Wang, H. Peng, J. Li, and Y. Peng, *J. Ceram. Process. Res.* 18 (2017) 116-121.
- K. Liu, W. Song, Y. Xu, J. Li, and Z. Wang, *J. Ceram. Process. Res.* 19 (2018) 146-149.
- W.K. Jung, J.W. Hong, and D.H. Choi, *J. Ceram. Process. Res.* 22 (2021) 86-90.
- M.R. Bodke, Y. Purushotham, and B.N. Dole, *J. Ceram. Process. Res.* 16 (2015) 601-604.
- P. Kannappan and R. Dhanasekaran, *J. Cryst. Growth* 401 (2014) 691-696.
- M. Danilson, M. Altosaar, M. Kauk, A. Katerski, J. Krustok, and J. Raudoja, *Thin Solid Films* 519 (2011) 7407-7411.
- M. Tsega, F.B. Dejene, and D.-H. Kuo, *J. Alloys Compd.* 642 (2015) 140-147.
- Y. Wu, Y. Zhang, Y. Sui, Z. Wang, S. Lv, M. Wei, Y. Sun, B. Yao, X. Liu, and L. Yang, *Ceram. Int.* 44 (2018) 1942-1950.
- S. Chen, M. Cai, and X. Ma, *J. Alloys Compd.* 689 (2016) 36-40.
- L. Yuan, A. Han, M. Ye, X. Chen, C. Ding, and L. Yao, *Sol. Energy* 163 (2018) 453-460.
- T.R.A. Thara, P.P. Rao, A.K.V. Raj, and T.S. Sreena, *Sol. Energy Mater. Sol. Cells* 200 (2019) 110015.
- A.K.V. Raj, P. Prabhakar Rao, S. Divya, and T.R. Ajuthara, *Powder Technol.* 311 (2017) 52-58.
- B. Huang, Y. Xiao, H. Zhou, J. Chen, and X. Sun, *ACS Sustain. Chem. Eng.* 8 (2018) 10735-10741.
- L. Sandhya Kumari, P. Prabhakar Rao, A. Narayana Pillai Radhakrishnan, V. James, S. Sameera, and P. Koshy, *Sol. Energy Mater. Sol. Cells* 112 (2013) 134-143.
- T.R. Aju Thara, P.P. Rao, S. Divya, A.K.V. Raj, and T.S. Sreena, *ACS Sustain. Chem. Eng.* 5 (2017) 5118-5126.